The Astrophysical Journal, 810:98 (13pp), 2015 September 10 doi:10.1088/0004-637X/810/2/98

OBSERVATIONS OF AN ENERGETICALLY ISOLATED QUIET SUN TRANSIENT: EVIDENCE OF QUASI-STEADY CORONAL HEATING

N. Brice Orange[1,2], David L. Chesny[1,3], and Hakeem M. Oluseyi[3,4]
[1] OrangeWave Innovative Science, LLC, Moncks Corner, SC 29461, USA
[2] Etelman Observatory, St. Thomas, United States Virgin Islands 00802, USA
[3] Department of Physics & Space Sciences, Florida Institute of Technology, Melbourne, FL 32901, USA
[4] Department of Physics, Massachusetts Institute of Technology, Cambridge, MA 02139, USA
Received 2015 January 21; accepted 2015 July 27; published 2015 September 3

ABSTRACT

Increasing evidence for coronal heating contributions from cooler solar atmospheric layers, notably quiet Sun (QS) conditions, challenges standard solar atmospheric descriptions of bright transition region (TR) emission. As such, questions about the role of dynamic QS transients in contributing to the total coronal energy budget are raised. Using observations from the Atmospheric Imaging Assembly and Heliosemic Magnetic Imager on board the *Solar Dynamics Observatory*, and numerical model extrapolations of coronal magnetic fields, we investigate a dynamic QS transient that is energetically isolated to the TR and extrudes from a common footpoint shared with two heated loop arcades. A non-causal relationship is established between episodic heating of the QS transient and widespread magnetic field re-organization events, while evidence is found favoring a magnetic topology that is typical of eruptive processes. Quasi-steady interchange reconnection events are implicated as a source of the transient's visibly bright radiative signature. We consider the QS transient's temporally stable (≈35 minutes) radiative nature to occur as a result of the large-scale magnetic field geometries of the QS and/or relatively quiet nature of the magnetic photosphere, which possibly act to inhibit energetic build-up processes that are required to initiate a catastrophic eruption phase. This work provides insight into the QS's thermodynamic and magnetic relation to eruptive processes that quasi-steadily heat a small-scale dynamic and TR transient. This work explores arguments of non-negligible coronal heating contributions from cool atmospheric layers in QS conditions and contributes evidence to the notion that solar wind mass feeds off of dynamic transients therein.

Key words: Sun: atmosphere – Sun: chromosphere – Sun: corona – Sun: magnetic fields – Sun: transition region

1. INTRODUCTION

Solar atmospheric activity has been directly tied to the underlying photospheric magnetic field evolution, which exhibits a wealth of complexity across broad spatial and temporal scales (e.g., Dowdy et al. 1986; Schrijver et al. 1992; Pevtsov et al. 2003; Uritsky & Davila 2012). Coronal magnetic field complexities are driven by enhanced magnetic energy and helicity build-up (Klimchuk 2006; Uritsky & Davila 2012); processes that are known to drive eruptive events like coronal mass ejections, jets, and flares (e.g., Solanki et al. 2006; Antiochos et al. 2007). However, the origin and physical relation of magnetic field complexities to observed multi-thermal solar atmospheric plasma responses remain a fundamental problem in solar physics.

The fine structure and dynamics of transient solar atmospheric phenomena (e.g., bright points (BPs), flares, jets, etc.) occurring across broad environmental conditions, i.e., active regions (ARs), to coronal holes (CHs), and temporal scales provide a direct utility for deciphering energy balance process (es) that are responsible for energizing and sustaining the hot outer solar atmosphere (Zacharias et al. 2011; Archontis & Hansteen 2014). Transient event observations indicate multi-thermal plasma compositions, as they are most often visible in multi-wavelength radiative imagery (e.g., Canfield et al. 1996; Madjarska et al. 2003; Lee et al. 2011; Orange et al. 2014b), and have revealed correlations with eruptive behavior, i.e., BPs with jets (Madjarska et al. 2012; Orange et al. 2014b). The current consensus is that transient events are self-consistent with flare models where magnetic reconnection serves as the central engine (e.g., Heyvaerts et al. 1977; Forbes & Priest 1984), but the nature of the magnetic environments and evolutions responsible for their formation remains unknown (e.g., Archontis & Hansteen 2014).

In relation to proposed self-similar generation mechanisms for transient events, evidence for energetically isolated counterparts (i.e., transition region (TR) BPs; Orange et al. 2014b) is of distinct interest, given the fact that their presence raises questions regarding the role of the varying thermodynamic conditions of the believed central engine, e.g., possible variations in the efficiency of magnetic reconnection (Longcope 1998; Longcope & Kankelborg 1999). Additionally, physical processes leading to the formation of dynamic transients with eruptive behavior, such as jets, are uniquely valuable. An inferred fundamental difference exists between jets and flares, as jets most commonly involve interchange reconnection between adjacent open and closed magnetic flux tubes (e.g., Shibata et al. 1992; Wang & Sheeley 1993; Wang et al. 1996; Shibata et al. 1997), and are considered responsible for their generation. Therefore, much stands to be learned from studies elucidating the radiative and magnetic field environments of energetically isolated transients and those with eruptive behaviors, especially in regard to deciphering the magnetic field's role in eruptive and non-eruptive processes in the presence of small-scale dynamic solar atmospheric transients.

Jets, which are most abundantly observed in CHs (e.g., Shimojo et al. 1998; Savcheva et al. 2007) and ARs (e.g., Shimojo & Shibata 2000; Schmieder et al. 2013), are most commonly linked to reconnection events between emerging and pre-existing fields (e.g., Yokoyama & Shibata 1995),

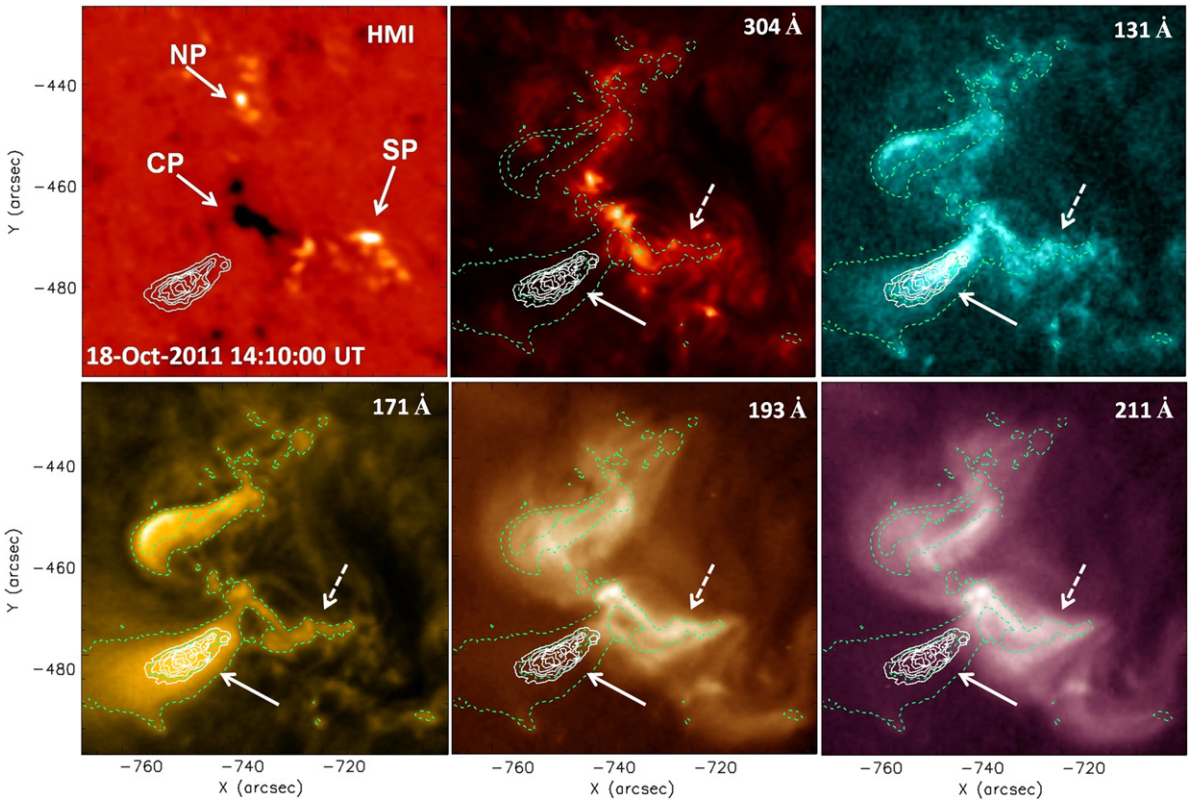

Figure 1. HMI LOS magnetogram and AIA radiative images, i.e., 304 Å, 131 Å, 211 Å, 193 Å, and 171 Å, from top right to bottom right in clockwise fashion, respectively, observed 2011 October 18 at 14:10 UT. The solid blue contours (also identified by a solid arrow) highlight the QS feature, visually bright at only TR temperatures, and distributed away from a common footpoint shared with two heated loop arcades. Note that the dashed arrow highlights one of these hot coronal loop arcades, while the CP, NP, and SP sites (as discussed in the text) have been identified on the HMI image.

where open magnetic fields are the key element in their collimated and evaporating plasma flows (e.g., Moreno-Insertis et al. 2008; Liu et al. 2009). To a lesser extent, they occur in regions of quiet Sun (QS), tending to be characterized by slower propagation speeds and shorter collimated outflows (Tate Arbacher et al. 2015), in contrast to those of CHs and ARs, and they correlate more often with BPs (Orange et al. 2014b; Tate Arbacher et al. 2015). Yokoyama & Shibata (1996) noted that some QS jets reflected loop brightenings due to a pair of opposing horizontal flows that resulted from the general geometry of the large-scale coronal magnetic fields, i.e., a larger horizontal component than that of CHs (Shibata et al. 1994). Similarly, Orange et al. (2014b) reported in a BP comparison study that a more horizontally directed current sheet (i.e., relative to the solar surface normal) explained the formation of a TR that was an energetically isolated QS BP, as a manifestation of self-similar plasma heating to its hotter coronal BP counterparts. The existence of evidence for the QS's capability of sustaining fine-scale structuring that is conducive to eruptive activity and coronal heating (Chesny et al. 2013) highlights the importance of identifying the fundamental processes leading to differing occurrence rates, and the general characteristics of eruptive events in CHs and ARs versus those of the QS.

In light of previous discussions, we have on hand a data set, derived from observations taken by the *A*tmospheric Imaging Assembly (AIA; Lemen et al. 2012) and the Heliosemic Magnetic Imager (HMI; Schou et al. 2012) on board the *Solar Dynamics Observatory* (*SDO*), that provides direct observational evidence of a previously unexplored, and possibly ubiquitous QS phenomena. Our QS transient event was energetically isolated to TR temperatures, and distributed away from two heated loop arcades to which it shared a common footpoint (Figure 1). Temporally analyzed radiative and line of sight (LOS) magnetic field imagery of the QS transient and immediately surrounding regions suggested that its visibly bright radiative signature derived from plasma heating via interchange reconnection events in an environment conducive to eruptive activity. Coronal magnetic field extrapolations are used as support for topologies that typically precede eruptive phenomena, i.e., a closed and open magnetic field interface. Based on the feature's temporally radiatively stable nature (≈35 minutes) physical sources are discussed that likely resulted in quasi-steady solar atmospheric energy redistribution over the large-scale eruptions that typically accompany such magnetic topologies.

2. OBSERVATIONS AND ANALYSIS

Observational data was obtained from *SDO*'s AIA and HMI instruments on 2011 October 18 from 14:05 to 14:40 UT (Table 1). The AIA data consists of the following passbands: 131 Å ($\log T \approx 5.8$), 171 Å ($\log T \approx 5.9$), 193 Å ($\log T \approx 6.2$), 211 Å ($\log T \approx 6.3$), and 304 Å ($\log T \approx 4.8$). It is recognized that AIA passbands are multithermal; however, in QS conditions the dominant emission observed in each passband originates from those reported above (O'Dwyer et al. 2010; Lemen et al. 2012). In support of such notions, we found that the typical flux rates associated with our observations

correlated with those measured from a large-scale QS region, close to Sun center, that was observed the same day.

Each AIA passband images the Sun's full disk approximately every 12 s and provides coverage of solar plasma from chromospheric to coronal temperatures, with a spatial resolution of $\approx 0\farcs6$. The HMI data are images of the full disk LOS magnetograms, with a cadence of 45 s and a spatial resolution of $\approx 0\farcs5$. AIA passband and HMI LOS magnetograms were pre-processed using standard Solar SoftWare (SSW), with pointing corrections of Orange et al. (2014a). Passband images were aligned at each time stamp via the SSW routine drot_map.pro and a visual correlation of bright coronal structures with strong photospheric magnetic elements, with a resultant uncertainty of $\approx 0\farcs6$ (Figure 1).

Recall that observational data was selected due to its witnessing of a visually bright QS feature at only TR temperatures (Figure 1). In relation to co-spatial underlying LOS magnetograms, this feature was distributed away from the the cusp of a horseshoe- like feature of photospheric magnetic elements, characterized by field strengths that were orders of magnitude larger than those of the surrounding background. The horseshoe magnetic feature, a higher order field configuration, was comprised of one strong negative and two weaker positive polarity elements. Note that the positive polarity elements lie in the positive solar x direction, relative to the negative element of the cusp position. Hereafter, the cusp position of the magnetic feature is referred to as the CP site, and the positive elements are referred to as the north and south positions, i.e., NP and SP sites, respectively (e.g., see Figure 1).

It is the goal of the this article to investigate the processes that supply the QS transient feature with heated plasma and maintain its visually bright radiative signature over an $\approx$35 minute period. Similarly, the role of the underlying magnetic field and two hot coronal loop arcades are probed, as they relate to the QS transient feature. We describe our methodology for investigating temporal variations of radiative and magnetic characteristics in Section 2.1. The techniques employed to investigate the associated three-dimensional (3D) coronal magnetic fields in the feature's vicinity are described in Section 2.2.

2.1. Radiative and Photospheric Magnetic Environments

The QS transient feature was characterized by a visibly bright radiative signature throughout our observational time domain, confined to AIA passbands dominated by emission lines formed at TR temperature regimes (i.e., 171 Å). Here we point out that throughout the remainder of this paper, the terminologies of chromospheric, TR, and coronal temperature regimes are used interchangeably for 304 Å, 171 Å, and 193 Å observations, respectively. To highlight the sub-structure of our QS transient feature, we first obtained an average image, per AIA passband, over the entire duration of our presented observation sequence (i.e., 14:05 UT–14:40 UT). Subsequently, this average image (baseline) was then subtracted off from all imagery, per respective passband. In that respect, our methodology utilizes radiative images that are less than their respective image average (covering the $\approx$40 minute time domain) to physically highlight interesting sub-structures. In Figure 2 an example of this process has been provided. As shown in the figure, the QS transient was comprised of "loop-like sub-structures," e.g., see 14:25 UT in the figure. Visual inspection revealed that these structures experienced multiple heating and cooling episodes (i.e., brightenings and dimmings, respectively), while their footpoints, opposing those shared with the hot coronal loop arcades, brightened in chromospheric emission through coronal emission (Figure 2). Note that for simplicity, throughout the remainder of this paper, the aforementioned loop structures are referred to as the "north" and "south" loops, NL and SL, respectively.

In regard to the previously highlighted "heating and cooling" episodes, it should be recognized that our use of AIA filtergrams does not allow an explicit determination of whether or not such intensity increases are a result of plasma heating or the result of the presence of dense warm material (Chandrashekhar et al. 2014). However, we emphasize that in relation to coronal heating it remains essential to consider it not only a process of increasing temperature, but density as well (e.g., Aschwanden et al. 2007; Uzdensky 2007). To that effect, throughout the remainder of this paper, episodes of increasing radiative emission are referred to as "heating" events—a coronal heating supply either directly through plasma heating or enhanced plasma densities.

To investigate NL and SL radiative emission modulations we applied a semi-supervised tracing algorithm to 171 Å images that assigns a set of loop coordinates s along their spines (Orange et al. 2013). Loop tracings were then used to aggregate data from all remaining passbands, as well as to segment loops into sub-regions of their common footpoint shared with the hot coronal loop arcades (i.e., CP site), opposing footpoint regions, and localized regions of radiatively enhanced TR emission (i.e., "bundle" regions). Here we note that the NL and SL segmentations were performed via a combination of the visual inspection of image-average-subtracted observations and their cross-correlation with loop-cross-section-smoothed radiative fluxes as a function of s, with errors derived from photon-counting statistics (e.g., Figure 3). Light curves for segmented regions were then generated by integrating the 3σ brightest flux, minus the running average, and standard error prorogation techniques.

As highlighted previously, we wish to study the possible role of the higher order underlying magnetic field configuration in our QS transient's heated plasma supply; particularly, this is the LOS magnetic field of the NP, SP, and CP sites, identified above. The selection of these magnetogram regions throughout our observational time domain is detailed as follows. First, at the onset of our observation sequence (14:05 UT), the magnetogram, with 171 and 193 Å intensity contours overlaid (e.g., similar to that presented in Figure 1), was visually inspected and utilized to define the three footpoint regions highlighted by the contoured intensity isolines. Then at each of the footpoint sites, a boxed region was defined that encompassed the corresponding photospheric magnetic element, as well as some surrounding background. Throughout the remainder of our observation sequence, at approximately one minute intervals, similar visual inspection techniques were employed, in order to minimize instances of false emergence, cancellation, or fragmentation events due to magnetic flux movement out of or into the selected fields of view (FOVs).

Temporal variations in the unsigned magnetic flux $|\Phi|$ were then measured from an integration of the positive and negative flux elements in the above described NP, SP, and CP regions, with errors propagated from photon-counting statistics (Figure 4). Within each region, magnetic flux densities ($\rho_B^{\pm}$), which are defined as the number of positive and negative flux

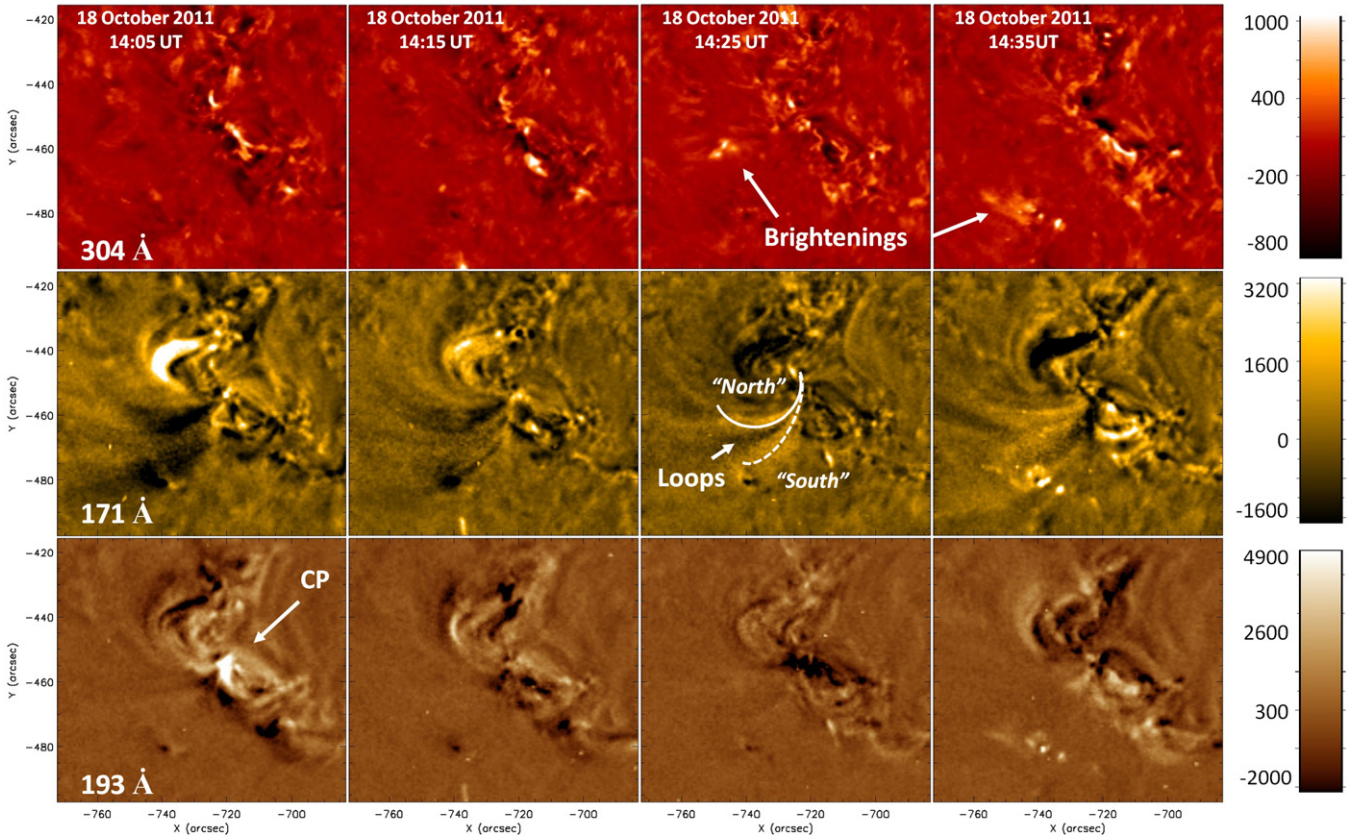

Figure 2. The 304 Å, 171 Å, and 193 Å images (DN pixel^{-1} s^{-1}), minus image averages, from top to bottom, respectively, observed on 2011 October 18, covering 14:05 UT–14:35 UT at approximately 10 minute intervals, from left to right, respectively. In these images we have highlighted the CP site, as well as some physically interesting sub-structures of the QS transient feature that were revealed during this process, namely the appearance of "loop-like" structures and small-scale brightenings.

elements above and below a threshold of 20 G (DeForest et al. 2007; Uritsky & Davila 2012), i.e.,

$$\rho_{|B|} = \frac{\sum_N I(|B|)}{N}, \tag{1}$$

where N is the number of pixels in the FOV, $|B|$ is the LOS magnetic field, and $I(|B|)$ is an indicator function defined as

$$I(|B|) = \begin{cases} 1, & |B| > 20\ \mathrm{G} \\ 0, & \text{Otherwise}, \end{cases} \tag{2}$$

were additionally measured (Chesny et al. 2013; Orange et al. 2013). Note that these results allow investigations of whether and how flux likely contributes to reconnection events (Sakai et al. 1997; Chesny et al. 2013; Orange et al. 2013). Additionally, magnetic flux densities were used as a means for estimating photospheric magnetic flux imbalances, $\psi_{|\rho|}$, relative to the CP from the NP and SP sites, i.e.,

$$\psi_{|\rho|}^{\mathrm{NP,SP}} = \frac{\rho_B^{\mathrm{NP,SP}} - \rho_B^{\mathrm{CP}}}{\rho_B^{\mathrm{CP}}}. \tag{3}$$

Uncertainties in both magnetic flux densities and their respective gradients were derived from a combination of photon-counting statistics and standard error propagation techniques. We recognize that there is not a real flux imbalance, and that such measurements are strongly influenced by both the region from which the measurement is derived, as well as those below our applied threshold. As such, we emphasize that our $\psi_{|\rho|}$ measurements are only used as a qualitative assessment of the general magnetic system, and that the fluxes therein likely contribute to reconnection processes, where our QS transient was witnessed.

2.2. Coronal Magnetic Field Environment

The coronal magnetic field environment of our QS transient was investigated by employing the Coronal Modeling Software (CMS; van Ballegooijen 2011, private communication). The CMS, written in the Interactive Data Language and Fortran90, describes the 3D coronal magnetic structure as a function of a single instant in time using the nonlinear force-free method, (e.g., van Ballegooijen et al. 2000; Mackay & van Ballegooijen 2006) to extrapolate coronal magnetic fields from observations of the LOS magnetic photosphere. The CMS deduced that coronal magnetic field models rely on a HMI LOS magnetogram, serving as a lower boundary condition, and a synoptic optical long-term investigations (Keller 1998) Carrington rotation map describing the full solar disk photospheric magnetic field for the computation and construction of a global potential field model. Each resultant empirical field model is comprised of a high- and lower-resolution area, which both depend on spherical coordinate systems, i.e., r, θ, ϕ, where r is the radial distance from the Sun's center, θ is the angle relative to the axis of solar rotation, and ϕ is the azimuthal angle.

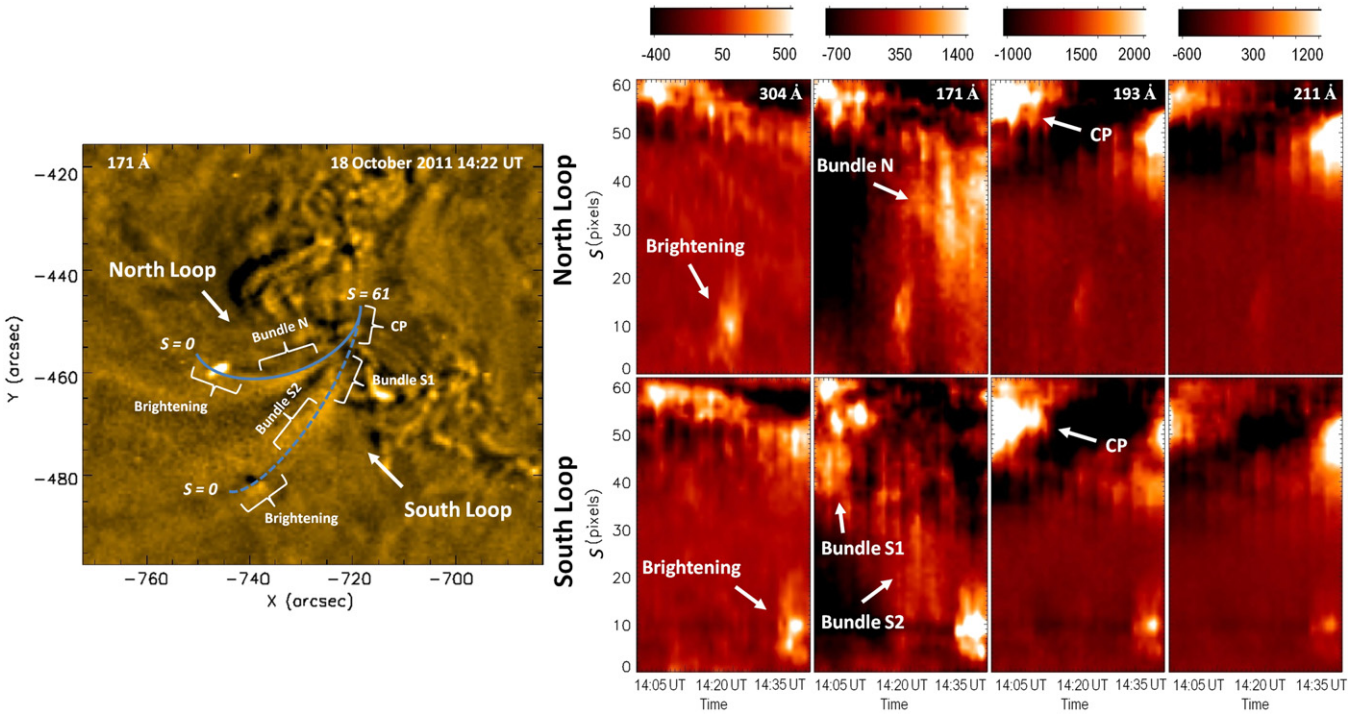

Figure 3. Left: 171 Å radiative image observed on 2011 October 18 at 14:22 UT, with solid (blue) and dashed (blue) lines marking the spines of the NL and SL features, respectively. Additionally denoted are the CP site, bundles, and brightening segmented regions of each feature, as discussed in the text. Right: radiative fluxes (DN pixel^{-1} s^{-1}), minus image averages, smoothed as a function loop spine position, s, for the NL and SL features (top and bottom rows, respectively) vs. time for 304 Å, 171 Å, 193 Å, and 211 Å observations on 2011 October 18, covering 14:05 UT–14:40 UT at approximately one minute intervals, from left to right, respectively. In these images we have also highlighted the CP site (same for both features), brightenings, and bundle regions that are indicative of localized heating for each feature.

The high-resolution (HIRES) region represents a discrete volume, large enough such that accounting for spherical geometry is required. In our case, the HIRES volume reflects a lower boundary area defined by an HMI LOS magnetogram extending to a height, Z, at which the field lines become radial, i.e., $Z > R_{\odot}$. Potential magnetic fields of the HIRES regions are computed using spherical harmonics and eigenmode solutions, where the HIRES boundary (i.e., that with the lower-resolution region) is satisfied by a continuous normal magnetic field component. Everywhere in the HIRES volume, the magnetic field is defined by,

$$\boldsymbol{B} = \nabla \times \boldsymbol{A}, \tag{4}$$

with $\boldsymbol{A}$ as the vector potential field, such that,

$$\nabla \cdot \boldsymbol{B} = 0, \tag{5}$$

is satisfied, while initial non-potential field conditions are setup from a flux rope insertion to potential fields and then subsequently relaxed using magnetofrictional relaxation techniques. Note that variable grid spacing is used within this region to make possible the construction of models that extend to large coronal heights. The lower-resolution region, referred to as the global region, is represented by a current-free potential field, derived using uniform grid spacing and the synoptic map of the radial magnetic field in the photosphere.

The radial components of the magnetic field, B_r, in the HIRES and global regions are defined initially by the lower boundary photospheric observations of the magnetograms and synoptic maps, respectively. Then the potential field $\boldsymbol{B}(\boldsymbol{r})$ associated with the observed photospheric flux distribution, $\tilde{B}_r(\theta, \lambda)$ at $r = R_{\odot}$ in spherical geometry, is calculated.

Note that the CMS coronal magnetic field models then allow field lines to be interactively traced, "visualized," by selecting specific flux elements in the photospheric FOV for which modeled results should be presented (i.e., field lines originating at that footpoint site). Here we emphasize that our interest in the CMS-generated 3D coronal magnetic field models lies in a qualitative assessment of the general field environment of our QS transient event. Thus, we restrict field model assessments to those that are supportive of our observations, e.g., Figure 5. Here we emphasize, as observed in Figure 5, that it supports previous indications that the QS transient was comprised of closed field structures (Section 2.1), and further suggests they are in close proximity to open fields.

3. RESULTS

Multi-wavelength AIA observations covering 14:05 UT – 14:40 UT revealed the QS transient event maintained its visibly bright nature, confined to TR temperature regimes, consistent with that observed in Figure 1. Similarly, the two loop arcades, in which the QS transient feature shared a common footpoint, were visually bright in TR and coronal images during our observational time frame. When analyzed in radiative imagery minus image averages, the QS transient feature provided evidence of localized episodes of heating and cooling, particularly in relation to the NL and SL structures (Figure 3). These localized "sub-regions," of both the NL and SL structures, have been identified in Figure 3, and their

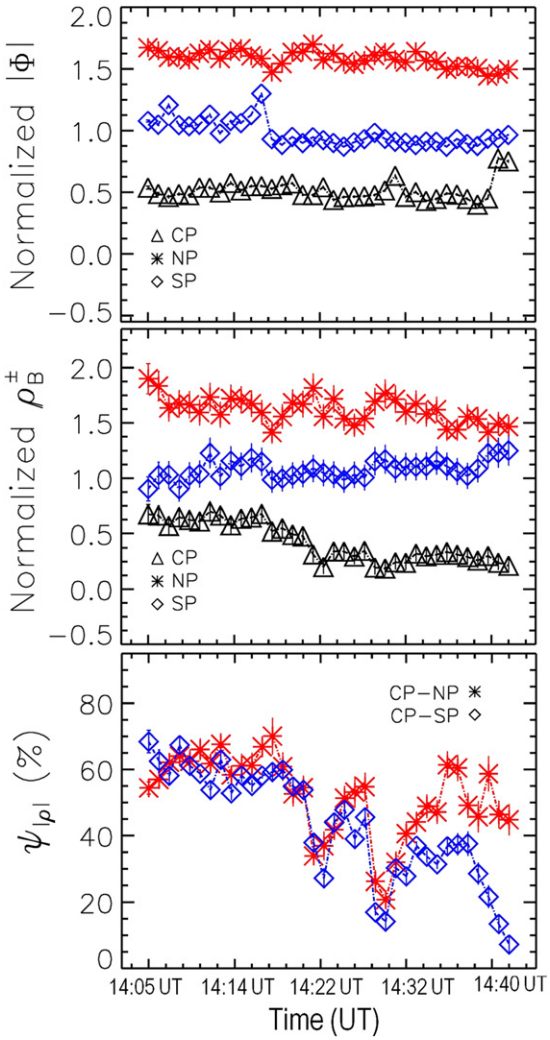

Figure 4. Unsigned magnetic flux (arbitrary units), flux densities (arbitrary units), and flux density gradients (%) from top to bottom, respectively, observed on 2011 October 18, over 14:05 UT–14:40 UT. Note that in the unsigned magnetic flux and flux density plots the data have been scaled for visualization purposes.

respective temporal radiative flux variations are presented in Figure 6, derived from techniques discussed in Section 2.1.

Investigations of the NL and SL sub-region radiative emission variations (Figure 6) and those of the underlying magnetic field (Figure 4), indicated the heating episodes exhibited a general similarity. This was widespread magnetic field modulations at the NP, SP, and CP sites (i.e., combination of emergence and cancellation), ≈2–4 minutes, preceded enhanced plasma emission of the CP site, and some variation of the NL and SL sub-regions, ≈3–4 minutes. Then, either or both of the NL and SL opposing footpoints brightened, which in some instances began in conjunction with the aforementioned heating events, ≈1–3 minutes. To that effect, the remainder of this section explicitly details the episodes during 14:05 UT–14:15 UT and 14:26 UT–14:40 UT to shed light on the dynamic heating that is likely the source of the QS transient feature's continually bright radiative nature. Table 2 lists event milestones that were witnessed during the aforementioned observational time-frames that will be reported on in detail below.

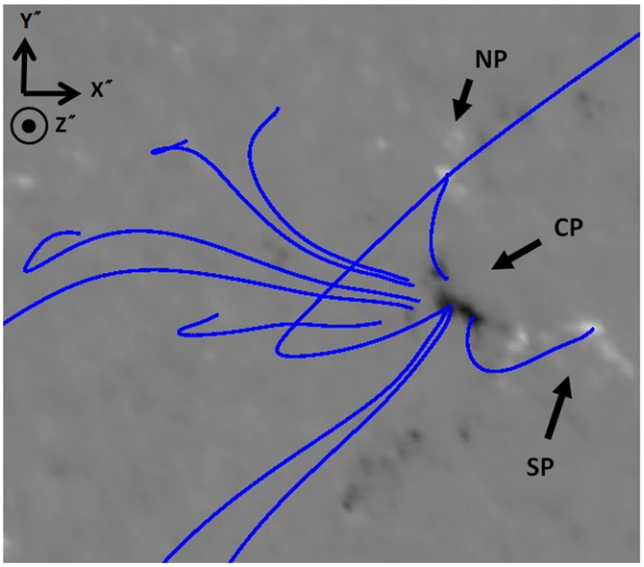

Figure 5. 3D CMS model of the coronal magnetic fields related to our QS transient feature, correlating with the 2011 October 18 14:15 UT LOS HMI magnetogram observation, and where the CP, NP, and SP sites have been identified therein.

The onset of the "first episode" (14:05 UT–14:07 UT) reported on here was accompanied by an approximately equivalent magnetic flux density decrease of ≈15% at both the NP and CP sites, while that of the SP increased by ≈7%. Similar trends of these sites' unsigned magnetic fluxes accompanied the previously described flux density modulations, i.e., the coupling of decreasing unsigned magnetic flux and flux density and vice-versa (Figure 4). Magnetic flux density gradients of the three sites, considered here as suggestive of the magnetic systems' energy balances, dropped by ≈10% between that of the CP SP, while the CP NP increased by ≈8%.

The CP, Bundle S1 (BS1), and Bundle N (BN) regions experienced radiative enhancements as the widespread magnetic field modulation ceased (Figure 6). Enhanced plasma emission of cooler atmospheric layers, i.e., the chromosphere and TR, were more pronounced at the CP site than that of the corona, particularly, for increasingly hotter coronal temperatures. However, the peak radiative emission at these cooler layers did lag behind that of the corona by ≈2 minutes. In relation to the localized NL event, chromospheric emission peaked prior to that of both the TR and corona. At the BS1 site, both coronal and TR enhancements preceded that of the chromosphere, whose subsequent peak occurred in conjunction with a second 171 Å emission-increasing episode, which was not witnessed in coronal passbands (Figure 6).

In Figure 7, the previously described localized heating of the SL is directly observed as a discernible spire-like structure, protruding from the CP site at ≈14:10 UT. As observed in accompanying 193 Å emission of this same figure, the 171 Å spire feature is extruding from a bright patch of coronal plasma, with a decreasing intensity distribution away from the CP site. By 14:11 UT, the spire-like structure has split, which is possibly evidence of an eruption (Liu et al. 2011a) into two disjointed bright patches. The lower portion that remained as a protrusion from the CP site slowly faded thereafter. The upper portion, i.e., that furthest from the CP site and only discernible

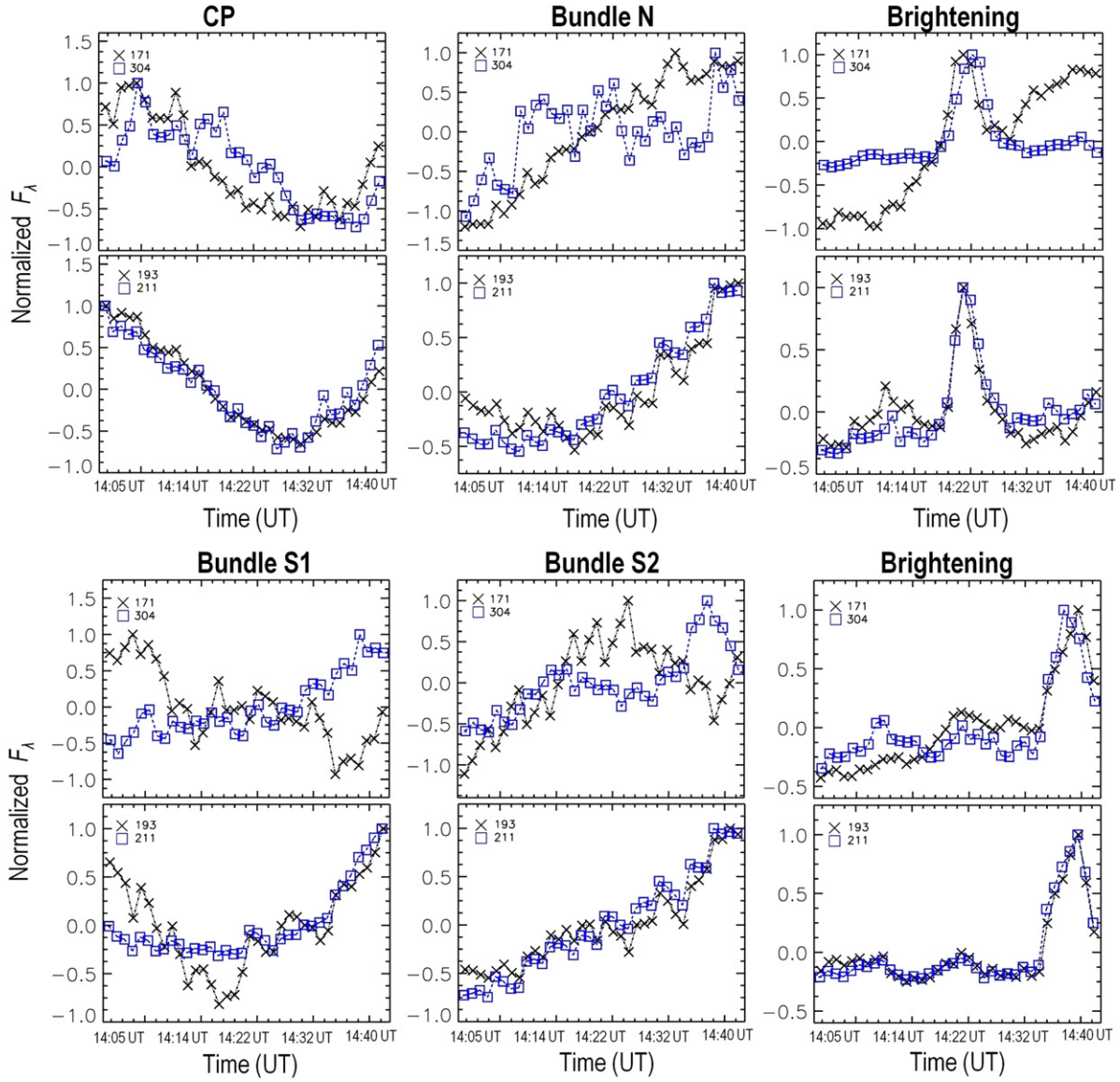

Figure 6. 3σ brightest fluxes (arbitrary units) of the NL and SL segmented regions (top and bottom panels, respectively) identified in Figure 3, and labeled accordingly herein, vs. time for chromospheric through coronal passbands.

Table 1
AIA QS Transient Event Observations

Date	Time (UT)	Solar Coordinates (X, Y)
2011 Oct 18	14:05:00	−720, −455

in TR passbands, slowly fades, but additionally drifts outward, away from the possible eruption site, and southward. Interestingly, the upper portion's complete disappearance (i.e., 14:13 UT of Figure 7) coincides with the radiative peak of the SL's opposing footpoint, which was visually discernible in chromospheric emission through coronal emission. This feature then fades from view, first in chromospheric and coronal emission, followed by that of the TR.

During the 14:26 UT–14:28 UT "second episode" presented here, another widespread magnetic flux density modulation occurred (Figure 4). This instance entailed a CP site flux density cancellation of ≈20%, with emergencies of ≈12% and 9% at the NP and SP sites, respectively. Increased unsigned magnetic fluxes of the three sites accompanied the flux density modulations, however, are considered negligible here given their marginal enhancements ($\lesssim$10 G). Distinct decreases of magnetic flux density gradients that are correlated with this time interval (Figure 4) ≈30% between both that of the CP SP, and CP NP sites, which is consistent with the reported flux density trends.

As the above magnetic field event concluded, emission increases of the CP, SL, and NL bundled regions began (Figure 6). This CP site event lacked a chromospheric signature, while that of the BN region peaked first in the corona and then lagged to cooler atmospheric layers. Note that the BS1 radiative emission enhancements immediately following the magnetic field re-organization event were confined to TR and chromospheric regimes, but followed from an enhancement to coronal emission (only in 193 Å observations) that occurred in conjunction with the magnetic field event. In the BS2 region, radiative fluxes exhibited similar trends to those reported for the BN region in that coronal emission

Table 2
Event Milestones

Time	Milestone
Episode #1	
14:05–14:07	Magnetic cancellation at the CP and NP sites, emergence at the SP
14:06–14:09	Enhanced emission of CP and NL and SL bundles, which lags to cooler layers
14:11	SL loop ruptures—visually bright TR upper and lower bundle, later bright in the coronal regime; SL opposing the footpoint brightens
14:12	Upper TR bundle laterally drifts south, while both upper and lower bundles fade
14:13–14:14	SL opposing footpoint brightening peak, then completely faded
Episode #2	
14:26–14:28	Magnetic cancellation at CP site, SP and NP emergence
14:28–14:30	Enhanced emission of CP, and NL, and SL bundles, which lags to cooler layers
14:30	Spire-like structure in NL vicinity, more extended in TR
14:31–14:32	Lateral expansion of the TR spire, and evolving toward a more bundled appearance
14:32–14:33	Dimming of bundled plasma as it drifts north and outward (away from CP)
14:34	NL and SL opposing footpoints' radiative flux increases; the latter is only visually bright
Episode #3	
14:30–14:34	Magnetic cancellation at the CP site, and NP emergence
14:35–14:40	Enhanced emission of CP, and NL, and SL bundles; SL opposing footpoint peaks in chromosphere
14:37	Multiple spire-like structures in TR, mainly in the vicinity of the NL, and distinct (shorter) coronal counterpart
14:38	Shrinking of spire structures in TR; SL opposing footpoint peaks in TR and corona
14:39–14:40	Enhanced emission of CP, NL, and SL, again with TR spire-like structures discernible

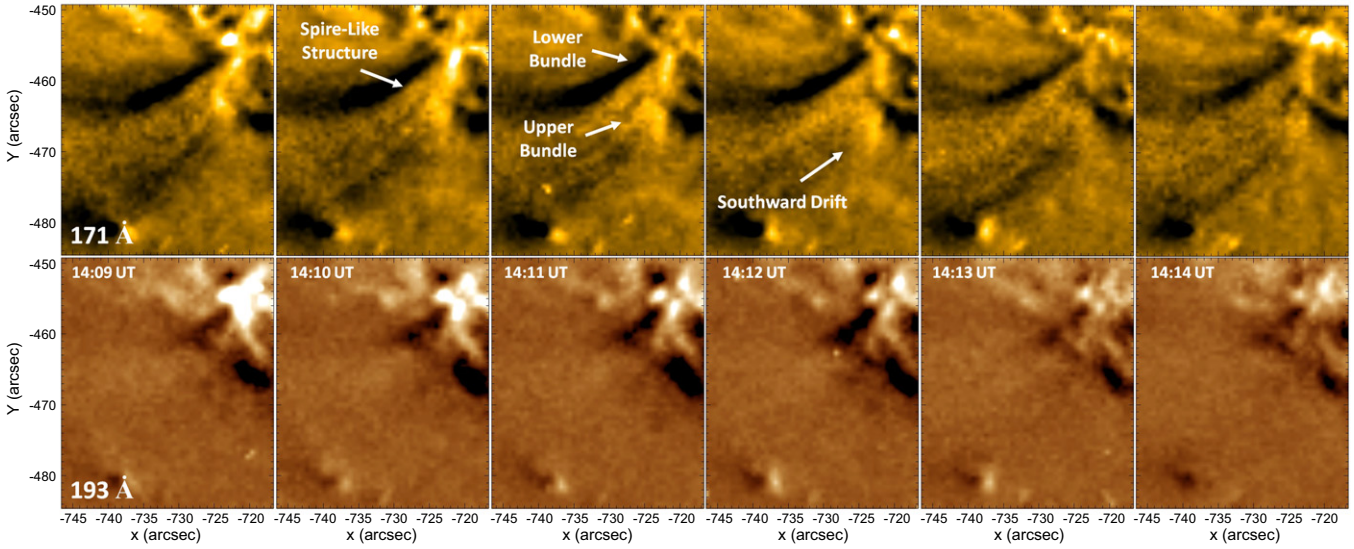

Figure 7. TR (171 Å) and coronal (193 Å), top and bottom rows, respectively, radiative images sequences, minus image averages, observed on 2011 October 18 during 14:11 UT–14:14 UT, covering the observational time frame correlating with our QS transients heating episode #1 as discussed in the text and outlined in Table 2. Note that here we have pointed out the appearance of a spire-like structure, which approximately one minute later appears to rupture into two distinct plasma bundles, with the upper portion drifting southward and cooling at later times.

peaked prior to that of cooler temperature regimes after the conclusion of the magnetic field re-organization event.

We emphasize that NL and SL bundle regions peaked in coronal emission at ≈14:30 UT and directly correlated with the onset of another spire-like structure (Figure 8). This feature was similar to that described for episode #1 (Figure 7), but with a more northward location, and was to a greater extent away from the CP site. Over the course of the next minute, this spire laterally expanded southward, as well as slightly increased in length. Additionally, as observed in Figure 8 a possible second spire-like structure has emerged, slightly southward of that of the first. At this time, we point out both spire-like structures, discernible at only TR regimes, and suggest that they are emanating from a bright, similar structure but a shorter coronal feature. The southward feature additionally hints at another possible eruption, i.e., a splitting into an upper and lower

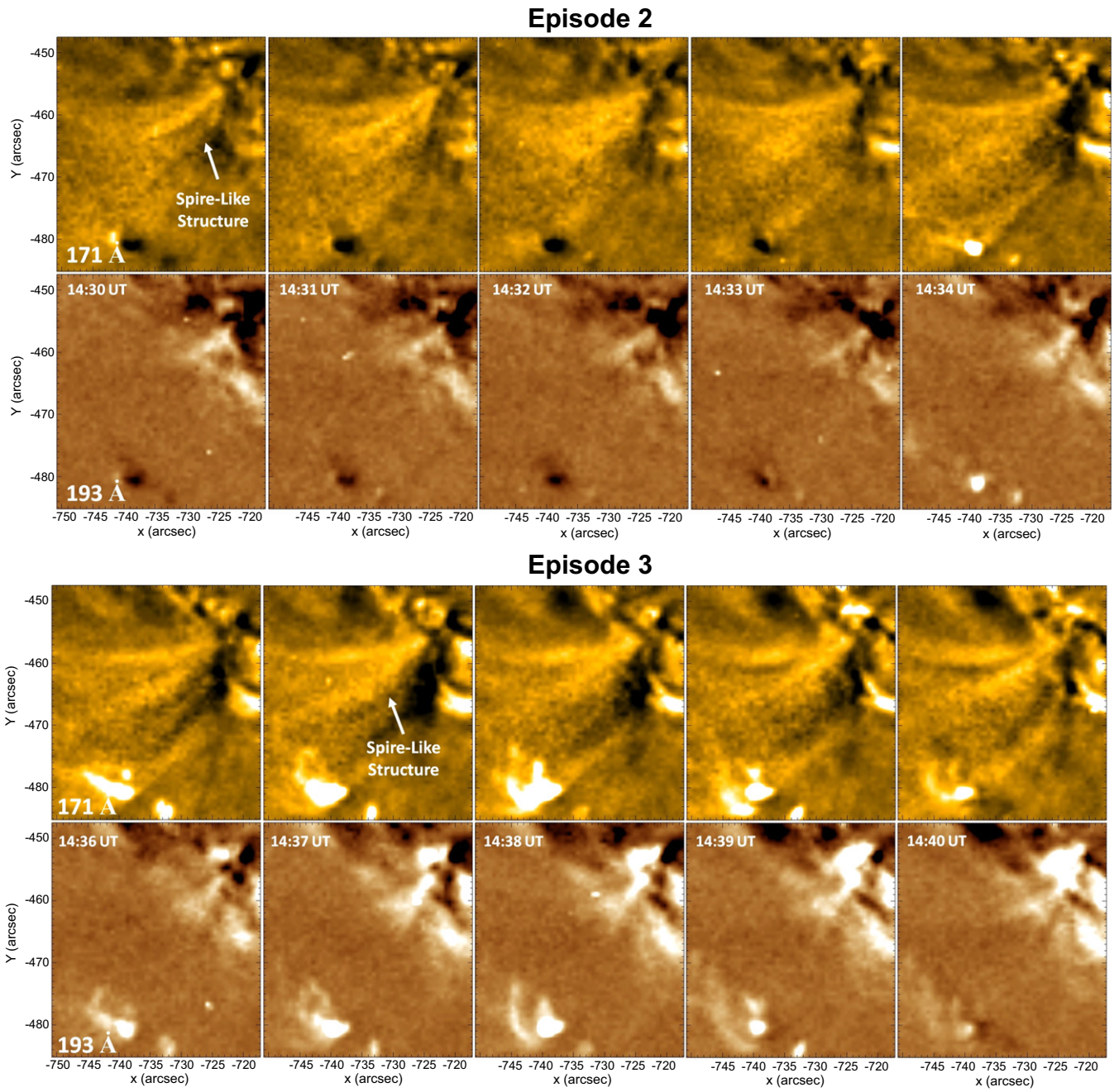

Figure 8. Radiative image sequences, presented as in Figure 7, but for our QS transient feature heating episodes #2 and #3 (top and bottom panels, respectively) as discussed in the text and outlined in Table 2. Note that in relation to each episode we have pointed out the appearance of a spire-like structure.

portion. Over 14:31 UT–14:33 UT, the previously bright TR emission of these structures, which is now more indicative of a single bright bundle of plasma and possibly a result of the previous evidence favoring an eruption, is observed to expand away from the CP site and dim. Here we speculate the enhanced radiative emission in the vicinity of the NL, by 14:33 UT (Figure 8), is likely evidence of said loop's apex (Liu et al. 2011a). By 14:34 UT the said upper TR plasma bundle has almost completely cooled and given rise to enhanced emission of the CP site and SL opposing footpoint, the latter of which was visually bright in chromospheric emission through coronal emission.

The remainder of our observation sequence, i.e., 14:34 UT–14:40 UT, is again indicative of another heating episode. As consistent with the previous ones, this episode starts with a magnetic field re-organization that is characterized by CP magnetic flux density emergence (≈12%) and NP cancellation (≈10%) that is followed by widespread emission enhancements of the CP, NL, and SL localized regions. Thus, below we detail the observed plasma dynamics, starting with the 14:36 UT observation time, which was previously pointed out above in Figure 8.

As observed at 14:36 UT in Figure 8, discernible bright TR patches exist in relation to our NL feature and in a similar

region as witnessed in episode #2 (i.e., see the 14:32 UT observations of same figure). Note that the opposing SL footpoint has peaked radiatively in chromospheric emission at this time (Figure 6). Again, consistent with previous episodes, the 14:37 UT observations indicate the appearance of another spire-like structure that protrudes from the CP site, and is confined to TR regimes expect for an accompanying, shorter, coronal counterpart. It is also pointed out at this time, slightly north of the previously described feature, the NL region presents evidence to a similar, possibly even more, collimated structure (Figure 8). Over the course of the following two minutes, the more southward spire-like structure of this episode has shrunk in length and dimmed, while the NL feature favors a similar evolution to that witnessed in each of the previous episodes, that is, the appearance of two distinct bright patches. In conjunction with these events, the SL's opposing footpoint radiatively peaks (Figures 6 and 8) though this time in TR and hotter atmospheric layers. By the conclusion of our observational sequence a number of sub-structures can be observed within our QS transient feature. To summarize, our 14:40 UT observations were characterized by enhanced radiative emission of various localized regions of the NL and SL features, and the re-emergence of a bundle of bright TR plasma, occurring in the region separating the two. These features again seemingly protrude from a common footpoint, visually bright in chromospheric through coronal emission, where coronal imagery supports a more compact spire-like structure.

4. DISCUSSION

Investigations of temporal radiative emission across large-scale solar atmospheric temperature gradients and co-spatial LOS magnetograms of our QS transient feature, as well as the CP site (i.e., footpoint shared with two hot coronal loop arcades) provide evidence for plasma heating as a result of widespread magnetic field re-organization events. It was pointed out in Figures 2 and 3 that the QS transient revealed a dynamic "sub-structure" composition. Detailed investigations (Section 3) indicated that the QS transient feature sub-structure was comprised of episodically heated (Figures 3 and 6) open and closed magnetic fields. Of distinct interest were the episodic heating events that exhibited a similar trend, which we summarize as follows.

Prior to each episode a re-organization of the underlying LOS magnetic environment of the QS transient feature (i.e., our CP, NP, and SP sites), such as emergence and/or cancellation of magnetic flux densities, was observed (Figure 4). Enhanced radiative emission at various localized regions, established in conjunction with the QS transient feature (i.e., the CP site, and/or NL and SL features), followed. Commonly the appearance of either a co-spatial, or adjacent spire-like feature, relative to either or both the NL or SL features (e.g., Figure 8), and/or the "splitting" of heated loop structures into two disjoint patches of bright emission (e.g., Figure 7), accompanied the localized radiative enhancements. Heating episodes concluded with enhanced radiative emission events of the opposing footpoints of either or both of the NL and SL features. In that respect, below we speculate the source of the episodic heating, and its relation to our QS transient feature's unique visibly bright radiative signature. Complementing these speculations are discussions of the general magnetic field environment and its temporal evolution, as they relates to our QS transient feature.

Evidence for loop rupturing and open magnetic fields are suggestive of interchange reconnection events (e.g., Madjarska et al. 2004; Krista et al. 2011) as well as reported widespread magnetic field emergence and cancellation events. Our observations of dynamically evolving bright plasma patches and the formation of spire-like structures following rupturing events are speculated as the occurrence of such reconnections, which leave in their wake newly opened and closed magnetic fields (e.g., Pariat et al. 2015). Spire-like structures that are supportive of an evaporating plasma flow (e.g., see 14:38 UT of Figure 8, possibly indicate injections of heated plasma into the QS transient feature, likely along newly opened magnetic field lines (e.g., Shibata et al. 1997; Shimojo et al. 2001; Pariat et al. 2015). Note that reported spire structures with visibly bright plasma distributions not decreasing away from the CP site (see 14:30 UT of Figure 8), and correlations with evolving bright plasma patches (see 14:10 UT of Figure 7) are inconsistent with such interpretations. We emphasize here that additionally the QS transient feature's radiative characteristics (Figures 1 and 9) starkly contrast such descriptions, i.e., those most common of "classical" jets (e.g., Allen et al. 1997; Shibata et al. 1997; Chandrashekhar et al. 2014).

Similarities of our observations to the chromospheric jet evolution detailed by Liu et al. (2011a), mainly, rupturing loops followed by two evolving bright plasma patches (e.g., 14:10 UT–14:12 UT in Figure 7), favor the fan-spine magnetic topology typical of jets, particularly the outer spine region (see Figure 1 of Liu et al. 2011a), where continuous injections of heated plasma occur along newly reconnected field lines, and lead to the formation of a diffuse bundle of bright emission (Liu et al. 2011a; Pariat et al. 2015), e.g., see Figure 9. Observed radiative emission enhancements near the conclusion of each heating episode, localized to regions out of the direct line of the diffuse bundle of bright 171 Å emission, are additionally considered here as supportive of a magnetic environment typical of jets. In relation to the fan-spine topology in 3D space, such events could indicate the dome structure as streamlines of falling material (Liu et al. 2011a), i.e., closed field structures (Figure 9). It is again emphasized that our QS transient maintains its radiative structuring and visibly bright TR signature over an ≈35 minute time frame, which as previously pointed out is in stark contrast to that which is typical of "classical" eruptive jets, as well as latter evolutions of the chromospheric jet study of Liu et al. (2011a). Below we postulate the source of our feature's unique and energetically stable radiative nature in a speculated magnetic field environment, where "classical" eruptive jets most commonly occur.

Episodic heating events, witnessed here on ≈3–5 minute intervals (Figure 6), and the QS transients visibly bright radiative signature over our observational time frame favor continuous type heating, with moderate reconnection rates (e.g., Pariat et al. 2010; Liu et al. 2011a; Pariat et al. 2015). The slower, quasi-steady reconnection rates and subsequent heating events would explain the lack of evidence in our observational data for high-speed injections, and significant torsional motion of the TR bundle, which is consistent with QS expectations (Tate Arbacher et al. 2015). It is speculated that such notions point to heated plasma injections, in relation to spire structures with decreasing intensity distributions away from the CP site, resulting from secondary thermodynamic processes (Shibata et al. 1997; Shimojo & Shibata 2000). In that respect, such

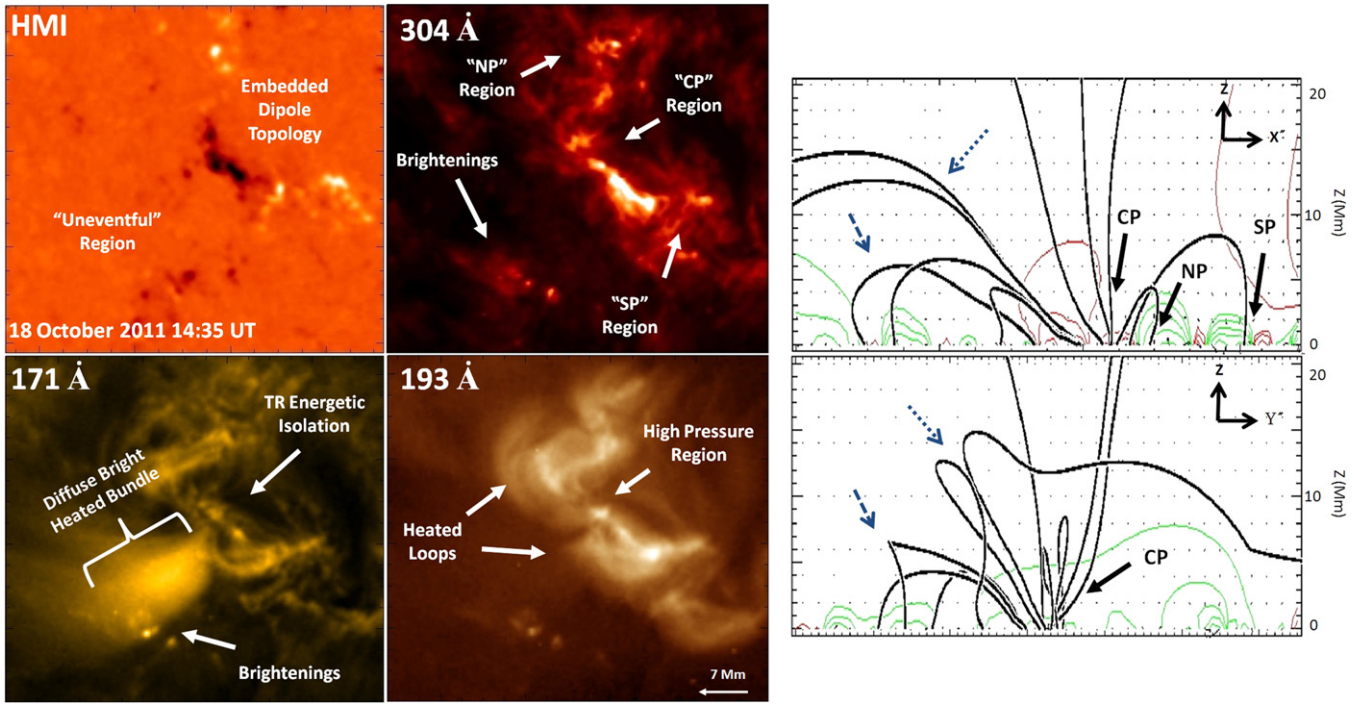

Figure 9. Left: HMI, 304 Å, 171 Å, and 193 Å images, from left to right and top to bottom, respectively. Throughout these images we have highlighted features that are extensively discussed in the text and pointed out physically interesting features that are supportive of a magnetic environment that is common for eruptive processes. Right: 3D CMS *X*–*Z* and *Y*–*Z* (top and bottom, respectively) cross slices of the modeled coronal magnetic field image presented in Figure 5. On these images the CP, NP, and SP sites have been identified, and the dashed and dotted (blue) arrows point to field lines that are suggestive of closed and open magnetic fields in the vicinity of our QS transient feature.

spire-like structure formation, which we emphasize includes observed collimated lower ends to ruptured loops, result from enhanced pressure and temperature gradients (e.g, Shimojo et al. 2001; Miyagoshi & Yokoyama 2003) at the CP site. We note, as highlighted above, that rupturing loop tops that spatially correlate with our QS transient feature's bundle of bright TR plasma (Figure 9), imply the deposition of additional heated plasma in the vicinity of the outer spine (Liu et al. 2011a). Therefore, both rupturing loop tops, and small-scale evaporation driven jets are speculated to be quasi-steadily supplying our QS transient feature with heated plasma; as such, heating events would explain its unique radiative signature (Figure 9).

In terms of our QS transient feature's energetically stable nature, and previous suggestions to a magnetic environment most commonly associated with jets, we speculate below to the lack of a dynamic evolution toward a classical eruptive jet. Recall, as pointed out in Section 1, jets most commonly occur in CHs and ARs, large-scale environmental conditions which differ significantly from that of the QS. In particular, CHs and ARs' jets align with open coronal magnetic fields, which in terms of ARs is consistent with the large spatial extent of closed field magnetic flux tubes that theoretically can be assumed as "open" (Shimojo & Shibata 2000; Schmieder et al. 2013), assumptions that possibly break down in QS regions, given the much shorter spatial extents, compared to ARs, of its overlying closed magnetic fields. Moreover, as supported by the works of Shibata et al. (1994) and Yokoyama & Shibata (1996), the QS environment possibly favors a fan-spine topology where the outer spine is more highly angled away from the solar normal, θ, based on the general geometry of the overlying coronal fields. Pariat et al. (2015) noted that for $\theta > 20°$ the outer spine actually connects to the side boundary of the fan plane, over the typical top boundary, and the resultant jet ejections would hit the closed side boundary. In that respect, speculations regarding such an atypical fan-spine topology of classical jets for our QS transient feature would explain the smearing of heated plasma that is more parallel to the solar surface, and the radiative structuring that is inconsistent with expectations (Shibata et al. 1994; Yokoyama & Shibata 1996; Orange et al. 2014b).

We hypothesize that the coupling of such a fan-spine topology with the general magnetic environment of our QS transient feature possibly acted to inhibit classical jet formation, particularly the instability build-up required to initiate a "breakout" fast reconnection phase (e.g., Hudson 2000; Pariat et al. 2009, 2015). First, the distributed geometry of the fan-spine, mainly the disjointed outer spine location and angle, could suppress the transition of the 3D null point into an extended current sheet that would be required for the formation of a straight jet (Pariat et al. 2015). Negligible results for strong magnetic emergence events, in direct relation to our QS transient feature, and torsional radiative motions, further support such a jet-inhibiting environment, as they are not indicative of a magnetic instability build-up, such as helicity injections (e.g., Schmieder et al. 1995; Canfield et al. 1996; Pariat et al. 2015). Moreover, our evidence pointing to the NP, SP, and CP sites as the potential predecessor of episodic heating to the QS transient feature (Figure 4) could also point to a draining away of their magnetic system's free energy through quasi-steady reconnections as plasma heating.

5. CONCLUSION

Using AIA and HMI observations that were recorded on 2011 October 18 during 14:05 UT–14:40 UT, a QS transient feature, energetically isolated in the TR that shared a common footpoint with two heated coronal loop arcades, and its LOS underlying magnetic field ,were studied. In radiative images, over our ≈35 minute observational time domain, the QS transient feature was composed of a diffuse bright bundle of TR heated plasma distributed away from the common footpoint shared with the heated loop arcades (Figure 9). The shared common footpoint site of our QS transient and two heated loop arcades, i.e., the CP region, was radiatively bright from the chromosphere through the corona during our observations as well. Radiative image investigations indicated that our QS transient was comprised of magnetically open and closed field structures (Figure 2), consistent with coronal magnetic field extrapolations (Figures 5 and 9) where episodic heating events resulted in dynamic evolutions of their radiative emissions (Figures 7 and 8). A general heating episode trend, derived from radiative and LOS magnetogram analyses, was established (Table 2) and explicitly detailed in Section 3.

Observational evidence, e.g., loop rupturing (Figure 7), spire-like structures (Figure 8), enhanced emission of the QS transient's opposing footpoints (Figure 3), and the embedded dipole of the underlying magnetic field (Figure 9), favored a magnetic topology typical of jets, i.e., fan-spine topology (e.g., Lau & Finn 1990; Pariat et al. 2010; Liu et al. 2011a; Pariat et al. 2015). It was considered, quasi-steady interchange reconnection events and thermodynamically driven small-scale injections were the source of our QS transient's heated plasma supply, and unique radiative structuring, i.e., a diffuse bright bundle of TR plasma (outer spine region; Liu et al. 2011a), distributed away from a single heated footpoint, where enhanced pressure and temperature gradients likely existed (e.g., Archontis et al. 2010; Orange et al. 2013; Chandrashekhar et al. 2014). We emphasize that quasi-steady QS transient heating events of ≈3–5 minutes,and negligible observational evidence for high-speed ejections and torsional motions favor moderate reconnection rates and evaporating plasma driven by secondary thermodynamic processes, respectively (e.g., Pariat et al. 2010; Shibata et al. 1997, respectively).

Though observations indicated magnetic topologies that are typical of large-scale eruptive phenomena, e.g., classical jets (e.g., Shibata et al. 1994; Canfield et al. 1996; Yokoyama & Shibata 1996; Shimojo et al. 2001), our QS transient maintained an atypical radiative structuring that is characteristic of such event-types. As such, discussions were presented suggesting that either or both of the QS conditions or the generally "uneventful" nature of the underlying magnetic photosphere possibly inhibited such a dynamic evolution. It was noted that the QS's general magnetic field geometry could have disrupted the typical fan-spine topology, where the outer spine was instead attached to a side boundary and characterized by a large degree of separation from the solar surface normal (Pariat et al. 2015), thus suppressing a catastrophic eruption where the material bundle evolves into a collimated jet (Liu et al. 2011a). Additionally, in relation to the general QS conditions, we point out that our transient's diffuse bright TR bundle, reflective of a "smearing" of heated plasma from a bright central core (Figure 9) is consistent with such QS field geometry interpretations. That is, previous works, e.g., Shibata et al. (1994), Yokoyama & Shibata (1996), Orange et al. (2014b), have described similar phenomena to result from a current sheet that is highly angled from the solar surface normal, i.e., more horizontally directed, as would be expected in our previously described scenario. We also speculated that the LOS magnetic photosphere's evolution and general strength was possibly unable to provide sufficient instabilities, such as through magnetic helicity injections, which are required to initiate a "breakout" phase (e.g., Pariat et al. 2009; Rachmeler et al. 2010; Liu et al. 2011a; Pariat et al. 2015).This was based on our observational evidence that favored quasi-steady reconnections that likely drained away significant portions of the magnetic system's free energy.

In summary, our work has provided significant insight regarding the environments that are most commonly associated with large-scale solar eruptions in the presence of the thermodynamic and magnetic conditions prevailing in the QS. Evidence presented here supports the QS's capability of sustaining eruptive topologies, but the accompanying energetic build-up processes are instead speculated to be resulting in quasi-steady coronal energy deposits over those required for the formation of a "breakout" or catastrophic eruption, which is characteristic of CHs and ARs. The observations presented indicate a quasi-steady upper TR and possibly lower corona interchange reconnections that are suggestive of temperatures where such magnetic to thermal energy conversions are occurring. In that respect, our work supports an elevated TR role in solar atmospheric energy redistribution processes, and possible solar wind mass feeding via localized quasi-steady coronal heating events. Finally, this work highlights the potential of future cooler atmospheric studies, in particular the TR, which can be considered the heights at which the solar wind originates (e.g., Parker 1963; Tu et al. 2005; Liu et al. 2011b) and where energetically isolated closed field structures have routinely been witnessed (Orange et al. 2013, 2014b; Orange 2014).

The authors greatly appreciate the reviewer's constructive comments on the manuscript. This research was supported by the National Aeronautics and Space Administration (NASA) grant NNX-07AT01G and the National Science Foundation (NSF) grant AST-0736479. N.B.O. was also supported by the Florida Space Grant Consortium, a NASA sponsored program administered by the University of Central Florida, grant NNX-10AM01H, as well as Christy and Arlene Orange. N.B.O. also thanks the University of the Virgin Islands. The authors also thank the Massachusetts Institute of Technology's Office of Provost, Physics Department, and Office of Equity and inclusion. Any opinions, findings, and conclusions or recommendations expressed in this material are those of the author(s) and do not necessarily reflect the views of the NSF or NASA.

REFERENCES

Allen, M. J., Oluseyi, H. M., Walker, A. B. C., Hoover, R. B., & Barbee, T. W., Jr. 1997, SoPh, 174, 367
Antiochos, S. K., DeVore, C. R., Karpen, J. T., & Mikić, Z. 2007, ApJ, 671, 936
Archontis, V., & Hansteen, V. 2014, ApJL, 788, L2
Archontis, V., Tsinganos, K., & Gontikakis, C. 2010, A&A, 512, L2
Aschwanden, M. J., Winebarger, A., Tsiklauri, D., & Peter, H. 2007, ApJ, 659, 1673
Canfield, R. C., Reardon, K. P., Leka, K. D., et al. 1996, ApJ, 464, 1016
Chandrashekhar, K., Morton, R. J., Banerjee, D., & Gupta, G. R. 2014, A&A, 562, A98
Chesny, D. L., Oluseyi, H. M., & Orange, N. B. 2013, ApJL, 778, L17

DeForest, C. E., Hagenaar, H. J., Lamb, D. A., Parnell, C. E., & Welsch, B. T. 2007, ApJ, 666, 576
Dowdy, J. F., Jr., Rabin, D., & Moore, R. L. 1986, SoPh, 105, 35
Forbes, T. G., & Priest, E. R. 1984, SoPh, 94, 315
Heyvaerts, J., Priest, E. R., & Rust, D. M. 1977, ApJ, 216, 123
Hudson, H. S. 2000, ApJL, 531, L75
Keller, C. U., & Nso Staff 1998, in ASP Conf. Ser. 154, Cool Stars, Stellar Systems, and the Sun, ed. R. A. Donahue & J. A. Bookbinder (San Francisco, CA: ASP), 636
Klimchuk, J. A. 2006, SoPh, 234, 41
Krista, L. D., Gallagher, P. T., & Bloomfield, D. S. 2011, ApJL, 731, L26
Lau, Y.-T., & Finn, J. M. 1990, ApJ, 350, 672
Lee, K.-S., moon, Y.-J., Kim, S., et al. 2011, ApJ, 736, 15
Lemen, J. R., Title, A. M., Akin, D. J., et al. 2012, SoPh, 275, 17
Liu, W., Berger, T. E., Title, A. M., & Tarbell, T. D. 2009, ApJL, 707, L37
Liu, W., Berger, T. E., Title, A. M., Tarbell, T. D., & Low, B. C. 2011a, ApJ, 728, 103
Liu, W., Ofman, L., Title, A. M., Zhao, J., & Aschwanden, M. J. 2011b, in AGU Fall Meeting Abstracts, A2043
Longcope, D. W. 1998, ApJ, 507, 433
Longcope, D. W., & Kankelborg, C. C. 1999, ApJ, 524, 483
Mackay, D. H., & van Ballegooijen, A. A. 2006, ApJ, 641, 577
Madjarska, M. S., Doyle, J. G., Teriaca, L., & Banerjee, D. 2003, A&A, 398, 775
Madjarska, M. S., Doyle, J. G., & van Driel-Gesztelyi, L. 2004, ApJL, 603, L57
Madjarska, M. S., Huang, Z., Doyle, J. G., & Subramanian, S. 2012, A&A, 545, A67
Miyagoshi, T., & Yokoyama, T. 2003, ApJL, 593, L133
Moreno-Insertis, F., Galsgaard, K., & Ugarte-Urra, I. 2008, ApJL, 673, L211
O'Dwyer, B., Del Zanna, G., Mason, H. E., Weber, M. A., & Tripathi, D. 2010, A&A, 521, A21
Orange, N. B. 2014, PhD thesis, Florida Institute of Technology
Orange, N. B., Chesny, D. L., Oluseyi, H. M., et al. 2013, ApJ, 778, 90
Orange, N. B., Oluseyi, H. M., Chesny, D. L., et al. 2014a, SoPh, 289, 1901
Orange, N. B., Oluseyi, H. M., Chesny, D. L., et al. 2014b, SoPh, 289, 1557
Pariat, E., Antiochos, S. K., & DeVore, C. R. 2009, ApJ, 691, 61
Pariat, E., Antiochos, S. K., & DeVore, C. R. 2010, ApJ, 714, 1762
Pariat, E., Dalmasse, K., DeVore, C. R., Antiochos, S. K., & Karpen, J. T. 2015, A&A, 573, A130
Parker, E. N. 1963, ApJS, 8, 177
Pevtsov, A. A., Fisher, G. H., Acton, L. W., et al. 2003, ApJ, 598, 1387
Rachmeler, L. A., Pariat, E., DeForest, C. E., Antiochos, S., & Török, T. 2010, ApJ, 715, 1556
Sakai, J. I., Ryutova, M., Schrijver, K., et al. 1997, in in Bulletin of the American Astronomical Society 29, ed. M. F. Bietenholz et al., 904
Savcheva, A., Cirtain, J., Deluca, E. E., et al. 2007, PASJ, 59, 771
Schmieder, B., Guo, Y., Moreno-Insertis, F., et al. 2013, A&A, 559, A1
Schmieder, B., Shibata, K., van Driel-Gesztelyi, L., & Freeland, S. 1995, SoPh, 156, 245
Schou, J., Scherrer, P. H., Bush, R. I., et al. 2012, SoPh, 275, 229
Schrijver, C. J., Zwaan, C., Balke, A. C., Tarbell, T. D., & Lawrence, J. K. 1992, A&A, 253, L1
Shibata, K., Ishido, Y., Acton, L. W., et al. 1992, PASJ, 44, L173
Shibata, K., Nitta, N., Matsumoto, R., et al. 1994, in X-ray Solar Physics from Yohkoh, ed. Y. Uchida et al. (Tokyo: Universal Academy Press), 29
Shibata, K., Shimojo, M., Yokoyama, T., & Ohyama, M. 1997, in ASP Conf. Ser. 111, Magnetic Reconnection in the Solar Atmosphere, ed. R. D. Bentley & J. T. Mariska (San Francisco, CA: ASP), 29
Shimojo, M., & Shibata, K. 2000, AdSpR, 26, 449
Shimojo, M., Shibata, K., & Harvey, K. L. 1998, SoPh, 178, 379
Shimojo, M., Shibata, K., Yokoyama, T., & Hori, K. 2001, ApJ, 550, 1051
Solanki, S. K., Inhester, B., & Schüssler, M. 2006, RPPh, 69, 563
Tate Arbacher, R., Tian, H., & Cranmer, S. R. 2015, in American Astronomical Society Meeting Abstracts 225, #13705
Tu, C.-Y., Zhou, C., Marsch, E., et al. 2005, Sci, 308, 519
Uritsky, V. M., & Davila, J. M. 2012, ApJ, 748, 60
Uzdensky, D. A. 2007, ApJ, 671, 2139
van Ballegooijen, A. A., Priest, E. R., & Mackay, D. H. 2000, ApJ, 539, 983
Wang, Y.-M., Hawley, S. H., & Sheeley, N. R., Jr. 1996, Sci, 271, 464
Wang, Y.-M., & Sheeley, N. R., Jr. 1993, ApJ, 414, 916
Yokoyama, T., & Shibata, K. 1995, Natur, 375, 42
Yokoyama, T., & Shibata, K. 1996, PASJ, 48, 353
Zacharias, P., Peter, H., & Bingert, S. 2011, A&A, 532, A112